Shock and Vibration 20 (2013) 503–518
DOI 10.3233/SAV-130764
IOS Press

Empirically bounding of space booms with tape spring hinges☆

A.L. Jennings*, J. Black and C. Allen[1]
Department of Aeronautics and Astronautics, Air Force Institute of Technology, WPAFB, OH, USA

Received 18 January 2012
Revised 29 August 2012
Accepted 21 November 2012

Abstract. Self-deploying structures seek to provide a compact launch package for large, lightweight satellite booms. One self-deploying method is a foldable tape spring. This paper examines the large scale behavior of a boom attached by a tape spring hinge during mock deployments. A boom attached by tape spring to a rigid stand was released and the boom bounced up to 60° before coming to rest (as opposed to snap-through behavior). These large amplitude bounces can cause the boom to collide with sensors, other booms or arrays causing damage or preventing full deployment. Results show the first bounce of deployment is nearly bounded by a four parameter ellipse. The ellipses of similar folds are similar also, suggesting that a model can be developed. Free-fall tests simulating the free-free condition found in microgravity also show similar elliptical motion. Envelopes that bound the extents of the boom motion allow for collisions to be prevented by adjustment of the design.

Keywords: Aerospace, space structures, deployment, empirical modeling, large deflection, nonlinear structures

1. Introduction

Limited cargo capacity and the prohibitive cost of in-space satellite assembly require that satellite booms must be deployed. Booms can be used for spars, solar panel arrays, antennas, and many other space applications. Boom deployments are either controlled or passive. Controlled deployments have a device, such as a driving motor or friction mechanism, that regulates the deployment. Uncontrolled deployments allow the boom to freely deploy after activation, typically by inflation or releasing a restraining pin or wire. A self-deploying boom can be folded into a stowed state such that the boom's elastic potential energy provides a sufficient restoring force to extend the boom to the deployed position. Using the elastic energy eliminates the need for a motor, which adds weight and increases energy requirements, or venting gas, which could disturb the orbit.

A tape spring has a transverse curve that can be flattened to fold or roll the tape spring, as shown in Fig. 1. The curve when deployed gives the structure a high stiffness resisting future folding. Elastic deployments typically have minimal damping and regions of low stiffness during the deployment. The initial strain energy can then cause large velocities, deflections and nonlinearities which can lead to catastrophic buckling and shocks. The traditional response is to add components to restrain the deployment to a quasi-static motion, but provide a possible failure point

*Corresponding author: A.L. Jennings, Department of Aeronautics and Astronautics, Air Force Institute of Technology, 2905 Hobson Way, WPAFB, OH 45433, USA. Tel.: +1 937 255 3636 ex7495; Fax: +1 937 656 4032; E-mail: Alan.Jennings@afit.edu.

☆The views expressed in this paper are those of the authors and do not reflect the official policy or position of the United States Air Force, Department of Defense, or the U.S. Government. This material is declared a work of the U.S. Government and is not subject to copyright protection in the United States.

[1]Present address: 1900 Founders Dr #300 Dayton, OH 45420, USA.

ISSN 1070-9622/13/$27.50

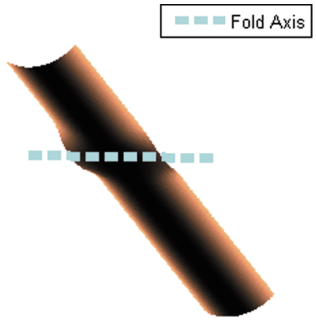

Fig. 1. The tape spring is concave except at the fold axis which can slide and rotate. The low stiffness about the fold axis allows for rotation.

and add to satellite mass and size. The mass and size of a satellite is growing in importance with the practicality of small satellites, such as CubeSats [1]. Models of self deploying booms are needed to better understand deployment dynamics and predict motion during deployment so collisions and binding can be avoided by redesigning the boom or folding pattern.

Folded structures can offer high accuracy for the final shape, but analysis of the deploying structure is complicated [2,3]. For large, flexible structures, care must be taken since otherwise minor disturbances could significantly impact performance [4]. The structure's folding pattern affects the success of deployment, and better patterns are not obvious [5]. Composite booms can be folded elastically or inflated and made rigid through curing epoxies [6,7]. Investigation of the final accuracy is shown in Ref. [8,9]. Alternatives to hinges are folded structures [2,3] or flattened booms, such as bi-STEM (storable tubular extensible member) [10,11], and coilable booms [12]. Boom design is an active research direction with new boom designs and deployment methods such as miniaturizing tape spring booms for CubeSat applications [13], inflated tape spring structures [14,15] and new coilable configurations [16].

In-depth analysis of specific tape springs folds has previously been performed, often based on principles of shell theory in finite element analysis (FEA) [17,18]. Analysis is complicated by dynamics and snap-through behavior causing ill-conditioned models [19]. Testing has focused primarily on cases where the spring is directly folded over, though some experiments of diagonal folds have been investigated [20–22]. These studies involved metal tape springs while other testing has refined the use and manufacture of composite tape springs [23,24]. The selection of tape spring material may be dictated by component requirements, such as using conductive material, for antenna, or non-conductive material, to isolate sensors. The analysis presented here will provide a method to compare design choices based on the bound of deployment. The goal has been to determine the bending moment and torsion based on the folding and twisting of the tape spring [25]. Other work in the realm of characterizing boom properties has used frequency response to assess structural health [24,26].

Self-deploying hinges made from folded tape springs are currently being used. These hinges constrain the fold location and allow for the boom to be optimized for rigidity rather than the ability to fold [27,28]. Mathematical relationships of the bending and twisting moments to hinge angles are given in Ref. [29,30]. Hinges also allow for a paneling approach that is beneficial for arrays such as for sensors or solar panels [31,32]. Hinges can also be extended in 2 dimensions for self supporting reflector dishes [33]. A compromise example is the integrated, double-slot hinge. The slot through the boom allows the remaining sides of the hinge to function as a pair of tape springs [34]. The results of Ref. [34] allow for prediction of accuracy in the final shape and optimization of mass for 2-D deployments and simple 3-D deployments. Alternative to the integrated slot, combinations of tape spring pairs can attach at one edge, as the Triangular Rollable And Collapsible (TRAC) Boom, flaring open as a triangle or attached at both edges roughly forming a inner circle, as the lenticular boom also known as the Collapsible Tubular Mast (CTM) [35]. These geometries will have different tradeoffs in terms of packing volume, uniformity of stiffness and buckling load for a given length or weight.

Tape spring deployment buckling can be broadly classified into snap-through behavior, where the boom proceeds through the deployed position causing a fold in the reverse sense; or bouncing behavior, where the boom approaches the final position but then bounces back, creating a fold in the original sense. Snap through causes significantly higher stress, and has been the subject of material failure analysis. This work instead seeks to describe the large-scale motion. Both bouncing and snap-through behavior can create non-intuitive, large scale paths [18]. Better modeling

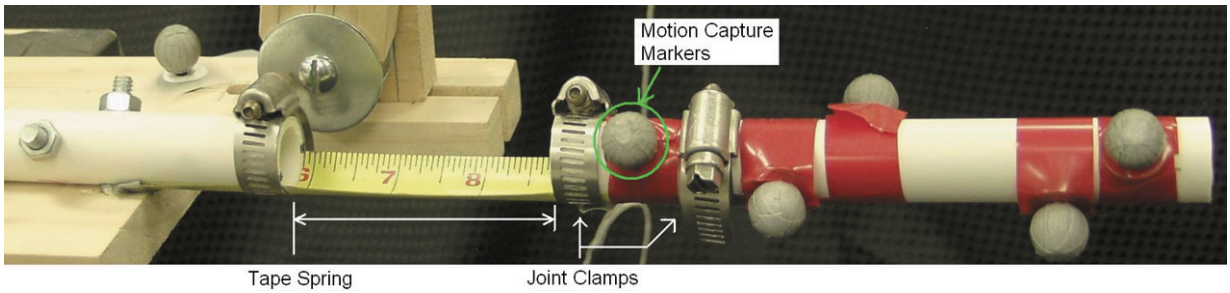

Fig. 2. The tape spring hinge was constructed by attaching a length of measuring tape between two tubes with clamps. Markers for the videogrammetry system are also attached to the free end.

of the large-scale motion is needed in order to predict 3-D position during deployment, and therefore predict binding and buckling of complicated structures.

This paper uses mock deployment data to identify the behavior of 3-D deployments, provide a parsimonious analysis of the motion and create a model to predict the first bounce of the deployment path. Typically individual tape springs are paired in parallel [32] or stacked with some spacing [34]. As a worst case analysis, only an isolated tape spring hinge was used to provide the largest lateral motion with the greatest uncertainty. The paper begins with a description of the equipment used. The analysis section explains how the deployment data is used to determine 1) a coordinate set based on joint properties, 2) the active degrees of freedom during a deployment and 3) a convenient parametrization of the deployment path can be parameterized. The results section shows how deployment paths are predictable based on similar initial folds and verifies that similar motion occurs in a free-free configuration.

2. Material and methods

For this work, a tape spring was connected to two rigid, massive booms.[1] A frame controlled the starting position of the deployment and provided a release mechanism for consistent results. This setup allowed for systematic testing of the factors that affect the path of deployment, such as: boom mass and moment of inertia, folding angle, twisting angle and direction of gravity. The pose of the free boom was measured by a 3 dimensional position and orientation during deployment with a high accuracy videogrammetry system. The following subsections will give the details of the joint construction, the test fixture and the videogrammetry system. Due to the number of coordinate systems used, each will be introduced in the final subsection.

2.1. Tape spring joints

The joint was constructed from lengths of 22 mm wide measuring tape (12.0 g/m), with 162 mm of 1/2" schedule 40 PVC pipe (21.34 mm outer diameter, 233 g/m), as shown in Fig. 2. The use of the pipe is meant to simulate the inertia of a long attached boom without adding substantial aerodynamic resistance. Each pipe had 50 mm of a double layer of the measuring tape (thickness of 0.10 mm each) fastened with two hose clamps[2] (18.3 g each) with a span of 76 mm between the ends of the boom (total length of 176 mm). The clamps provided a very stiff connection of the spring to the boom, though it did interfere with torsional alignment, but misalignment was less than 5°. The radius of the spring was slightly larger that of the tubing resulting in stiffness increasing towards the pipe. The increasing stiffness provides smooth feedback to keep the fold away from the boundaries. The side not being tested was fastened to the test stand. Five motion capture markers (2 g each) were placed on the free end at various locations.

[1] Massive and rigid as compared to the tape spring.
[2] SAE size #12, stainless steel.

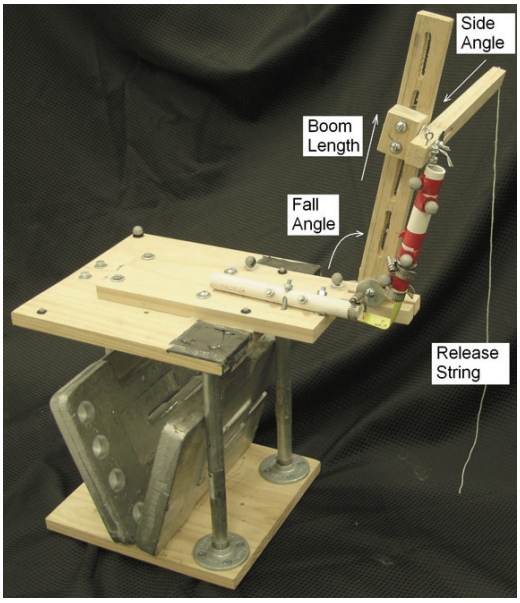

Fig. 3. The test stand allows for repeatable tests with a consistent start position and release.

2.2. *Testing fixture*

The purpose of the testing fixture was to limit the variation in release and not obstruct the view of the deployment to the videogrammetry system. The structure around the boom allowed adjustments for boom length, fall angle and angle of the boom to the side (see Fig. 3). Fixing the structure joints ensures the initial location of the free end could be repeated. The stationary end was attached by two sets of bolts at right angles to each other for high stiffness in all directions. For repeatability tests, deployment was activated by pulling a string which lifted a release pin. The pin release minimized occlusion of videogrammetry markers for higher accuracy, gave a more consistent starting position and made the release crisper than could be achieved by hand. When a wide variety of starting angles were desired, as opposed to a consistent start, the free end was held stationary and released by hand. Additional mass was added to the test stand base to decrease its vibration.

The hinge was aligned so that the ridges of the spring were within 5° of parallel to the base of the test fixture. The joint was then folded so that the free end would rotate up a set angle and be held by a pin through the tip of the tube. The fold angles could be approximately measured prior to analysis, but the actual angles measured via the videogrammetry system were used to categorize results. Results were recorded in batches of 15–25 deployments at a time. Multiple batches were taken for a test condition to prevent bias due to the setup.

2.3. *Videogrammetry system*

Three dimensional position measurement is accomplished by a videogrammetry system, also know as a motion capture system. Ten 16 megapixel cameras are mounted around the lab perimeter (similar to Fig. 4) for a working capture volume of approximately 5 m×7 m×2.5 m. These cameras are specially designed for videogrammetry and use near-infrared, strobed lights, bandpass filters and on-board processing to achieve high resolution realtime videogrammetry at 100 Hz. Retro-reflective, spherical videogrammetry targets of 3 mm to 13 mm diameter (as shown in Fig. 2) are marked to subpixel accuracy. The 2-D locations of marked targets on each image are sent to a central data station which interprets them as rays through space. Based on each camera's location and orientation, the global locations of the markers are found by ray intersection in the videogrammetry coordinate system, which is also used as the global coordinate system (GCS). Sets of 3-D target positions are compared to a library of objects. For each pattern match, the location and orientation of its body coordinate system is determined with respect to the GCS. Accuracy degrades from sub-millimeter, sub-degree accuracy as markers approach singularity conditions.

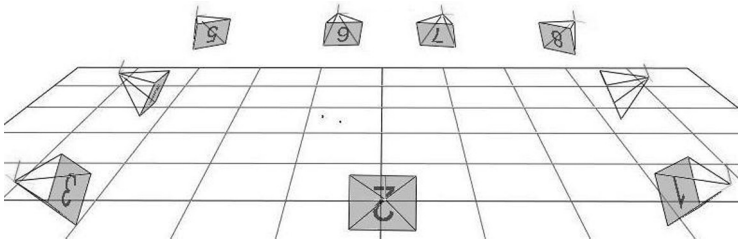

Fig. 4. Videogrammetry cameras are set up around the room's perimeter and track body motion.

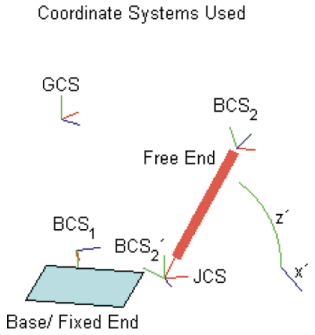

Fig. 5. Coordinate systems BCS_1 and BCS_2 give the rigid body motion of the fixed and free end respectively, in the global coordinate system (GCS). Coordinate systems JCS and BCS_2' are generated based on the motion of the free end. JCS is static while BCS_2' rotates with the free end. The z' and x' coordinates are a flattened cylindrical coordinate system used to describe the motion of deployment.

2.4. *Coordinate systems*

Coordinate systems are inherited from the measurement system or generated to describe deployments. Figure 5 shows an example with all the coordinate systems used. Data is collected from the videogrammetry system and is given in relation to an arbitrary global coordinate system (GCS). Each side of the joint is assigned a local coordinate system. The fixed end has an arbitrary body coordinate system (BCS_1). The free end has a coordinate system that lies near the axis of the boom, but the orientation of this coordinate system is arbitrary (BCS_2). The motion of the free end is used to create the location and orientation of the joint coordinate system (JCS). Co-located with the JCS, the BCS_2' rotates with the free end and is aligned to JCS when the free end is in the deployed position. The transform of JCS to BCS_2' is used to analyze the three rotation degrees of freedom, while the position of BCS_2 in BCS_2' gives the three translation degrees of freedom. The JCS is referenced to BCS_1 to account for relocation of the fixed end. The final coordinate system is a flattened cylindrical coordinate system to visualize and characterize the motion of deployment and will be defined in Subsection 3.2. Only two coordinates are needed: x' and z'.

3. Analysis

The tape spring hinge joint has multiple degrees of freedom (dof). A completely free joint has 6 dof to which mechanical attachments impose constraints. For the tape spring, stiffness is high in all translation directions and for inplane bending (4 dof). A tape spring begins concave except for near a fold axis shown in Fig. 1. The fold provides an axis for one rotational dof, but it is not constrained to a fixed position. The fold can rotate within the plane of the spring or slide axially along the spring. So the fold provides 3 dof: the distance of the fold from the fixed end, the angle of the fold axis and the rotation about the fold line. For a one-sided joint (opposed to a slot joint), the axial torsion stiffness typically must also be considered. In total, there may then be as many as 4 dof, but not all may be independent or expressed in natural deployment. Note that this represents the maximum number of independent degrees of freedom, and combinations of tape springs may have less depending on the configuration.

Rather than trying to directly measure these 4 dof, the 6 dof motion is analyzed for correlations between dof to determine the independent dof expressed during a deployment empirically. Body position and rotation is captured in an arbitrary, global coordinate system (GCS). The only requirement is that the body reference point for the deploying end (the origin of BCS_2) is near the axis of the deploying boom. To discriminate the motion into useful coordinates, a coordinate system based on rotations and translations of the joint (JCS) is developed in Subsection 3.1. Since the joint is fixed relative to the base, the transform from global to joint coordinates only needs to be developed once. In

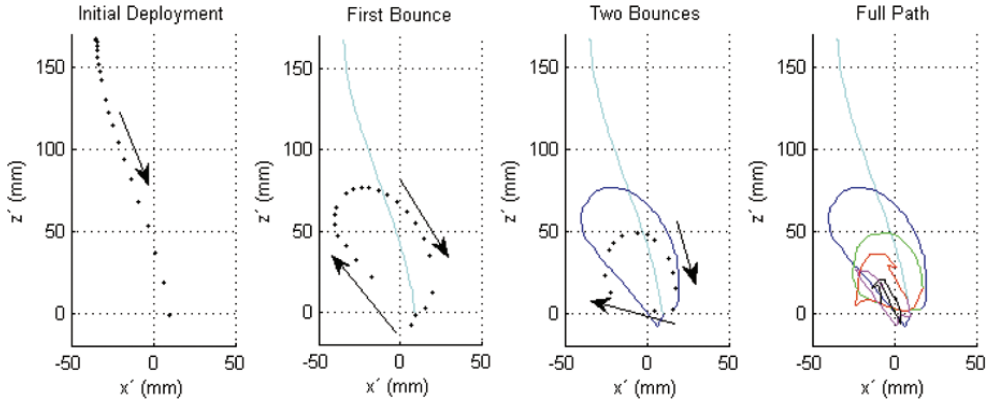

Fig. 6. The path data for a typical deployment with low lateral momentum, separated by bounces, is shown in the flattened cylindrical coordinates.

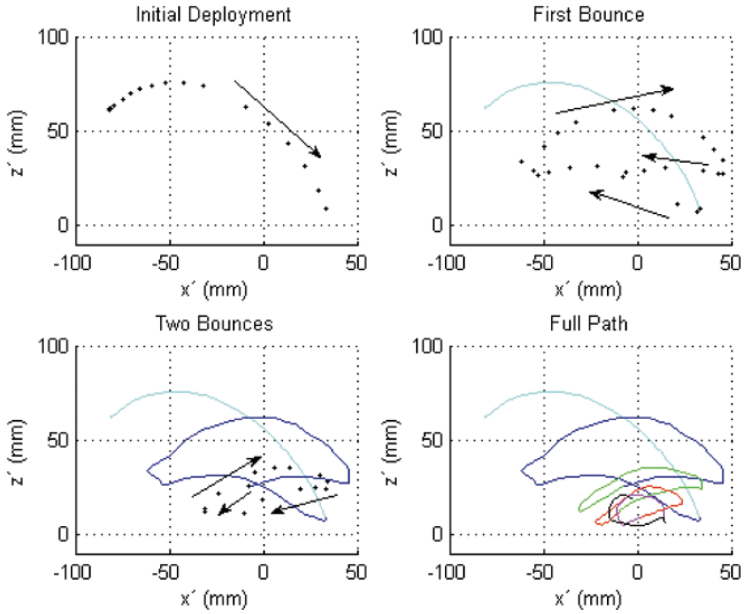

Fig. 7. The path data for a typical deployment with high lateral momentum, separated by bounces, is shown in the flattened cylindrical coordinates.

Subsection 3.2, the six dof will then be reduced to a parsimonious coordinate system (x', z') based on the manifold of poses during unforced deployment.

Deployments began in a folded position from which the free end would extend. The momentum of deployment would typically be stored as strain energy as the boom would come to a near stop when the boom is almost straight and the fold disappears. Snap-through behavior, where the boom over-rotates by creating a fold in the opposite sense; did not occur in the tests, was not the focus of this research and may need a different characterization. Instead, the strain energy would cause the boom to bounce back towards the starting point. Typically the bounce would be primarily vertical (with respect to joint), but sometimes more lateral. An example of vertical bounce is shown in Fig. 6 along with how the bounce diminishes and rounds out. Cases with large lateral momentum fold over to the opposite side of the yz JCS plane, as shown in Fig. 7 where the boom bounces sideways and diminishes. The goal of analysis is to find a polygon that can be used to determine the extents of the boom when it bounces back. This bound is an envelope of deployment used to determine the possibility of collision during the first bounce. Subsequent bounces typically are near the first bounce and have less kinetic energy. The folding design can then be adjusted until each boom's envelope is distinct so binding cannot prevent a successful deployment.

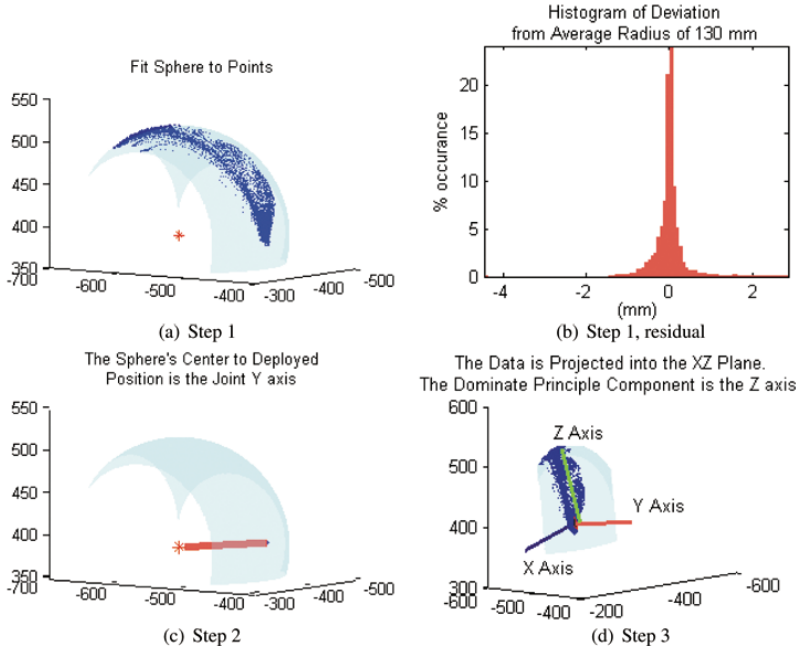

Fig. 8. Joint coordinates are developed by the position of the deployed end. Data comes from a set of near perpendicular deployments.

3.1. Joint coordinate system

The joint coordinates system is developed based on the motion of the free end as illustrated in Fig. 8. These coordinates provide the static frame from which the moving frame is referenced. First, the center of rotation of the joint is determined by a spherical fit. The deployed position is used as the primary direction reference while the remaining dominate principle component is used to determine the perpendicular to the tape spring plane.

The center of rotation of the joint is found by fitting a sphere to the origin of BCS_2 in the GCS. This is done in the least square of the squared distance error sense to provide a closed form solution [36].[3]

$$J = \sum_{i=1}^{I} \left((x_i - x_c)^2 + (y_i - y_c)^2 + (z_i - z_c)^2 - r_c^2 \right)^2$$

$$\begin{bmatrix} x_c \\ y_c \\ z_c \end{bmatrix} = \frac{1}{2} \begin{bmatrix} \sum_i x_i(x_i - \bar{x}) & \sum_i x_i(y_i - \bar{y}) & \sum_i x_i(z_i - \bar{z}) \\ \sum_i y_i(x_i - \bar{x}) & \sum_i y_i(y_i - \bar{y}) & \sum_i y_i(z_i - \bar{z}) \\ \sum_i z_i(x_i - \bar{x}) & \sum_i z_i(y_i - \bar{y}) & \sum_i z_i(z_i - \bar{z}) \end{bmatrix}^{-1} \begin{bmatrix} \sum_i (x_i^2 + y_i^2 + z_i^2)(x_i - \bar{x}) \\ \sum_i (x_i^2 + y_i^2 + z_i^2)(y_i - \bar{y}) \\ \sum_i (x_i^2 + y_i^2 + z_i^2)(z_i - \bar{z}) \end{bmatrix} \tag{1}$$

$$r_c = \sqrt{\frac{1}{I} \sum_{i=1}^{I} \left((x_i - x_c)^2 + (y_i - y_c)^2 + (z_i - z_c)^2 \right)} \tag{2}$$

where I is the number of data points, (x_i, y_i, z_i) is the i^{th} measurement of the origin of BCS_2, (x_c, y_c, z_c) is the center of the sphere, r_c is the radius and the bar notation, and $\bar{x}$, denotes the sample mean value.

The y axis is determined by the unit vector going from the sphere's center to the body point in the extended position. The z axis is perpendicular to the plane of the tape spring. Due to the out-of-plane flexibility, there is no well defined static pose. However, when the joint is folded directly over, the path remains close to the yz plane and is generally symmetric about the plane. The z axis is determined by the principle component of the motion in the

[3] This is different than the typical least square distance because the least squared distance does not provide a closed form solution. Implemented in MATLAB at http://www.mathworks.com/matlabcentral/fileexchange/34129.

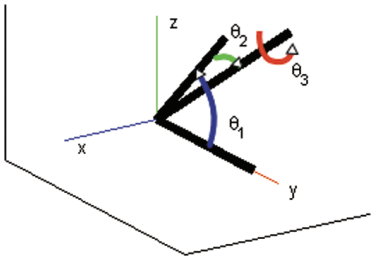

Fig. 9. The free end rotation is measured by a deployment angle, θ_1; a side angle, θ_2; and a twist angle, θ_3.

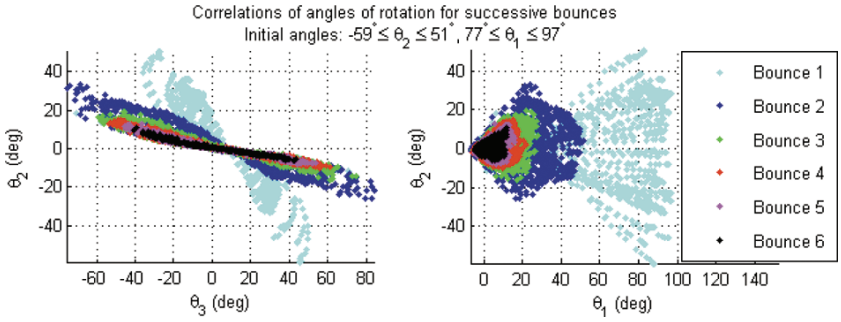

Fig. 10. Regular, significant motion was observed in the deployment angles as shown for deployments of ≈ 90° and side angles up to 60°. Translation was not significant, being uncorrelated and typically less than 3% of the nominal length.

xz plane for a set of perpendicular deployments. The direction of the z axis is chosen to be on the concave side of the joint. The x axis is chosen for a right hand coordinate system. These axis form the JCS and are referenced to the fixed end by BCS_1; so should the base be moved, the JCS can be found from the new fixed end pose. BCS_2' lies at the origin of JCS but rotates with the free end. When the free end is at the deployed position, BCS_2' is aligned with JCS.

Rotations of the free end are represented by a set of Euler angles for the rotation of BCS_2' into JCS. The first angle is based on the joint rotating up, next is a rotation for the side angle and finally a twist about the boom axis (1-3-2 convention). There are other choices for representing the boom rotations, but this was selected since it provides a useful decomposition as shown later. The three ordered rotations for a boom extending in the y direction are shown in Fig. 9. The equation for moving from body coordinates (u, v, w) to joint coordinates (x, y, z) is

$$\begin{bmatrix} x \\ y \\ z \end{bmatrix} = \begin{bmatrix} 1 & 0 & 0 \\ 0 & \cos(\theta_1) & -\sin(\theta_1) \\ 0 & \sin(\theta_1) & \cos(\theta_1) \end{bmatrix} \begin{bmatrix} \cos(\theta_2) & -\sin(\theta_2) & 0 \\ \sin(\theta_2) & \cos(\theta_2) & 0 \\ 0 & 0 & 1 \end{bmatrix} \begin{bmatrix} \cos(\theta_3) & 0 & \sin(\theta_3) \\ 0 & 1 & 0 \\ -\sin(\theta_3) & 0 & \cos(\theta_3) \end{bmatrix} \begin{bmatrix} u \\ v \\ w \end{bmatrix} = R_b \begin{bmatrix} u \\ v \\ w \end{bmatrix} \tag{3}$$

$$R_b = \begin{bmatrix} \cos(\theta_2)\cos(\theta_3), & -\sin(\theta_2), & \cos(\theta_2)\sin(\theta_3) \\ \cos(\theta_1)\sin(\theta_2)\cos(\theta_3)+\sin(\theta_1)\sin(\theta_3), & \cos(\theta_1)\cos(\theta_2), & \cos(\theta_1)\sin(\theta_2)\sin(\theta_3)-\sin(\theta_1)\cos(\theta_3) \\ \sin(\theta_1)\sin(\theta_2)\cos(\theta_3)-\cos(\theta_1)\sin(\theta_3), & \sin(\theta_1)\cos(\theta_2), & \sin(\theta_1)\sin(\theta_2)\sin(\theta_3)+\cos(\theta_1)\cos(\theta_3) \end{bmatrix} \tag{4}$$

where $(\theta_1, \theta_2, \theta_3)$ are the Euler angles. The Euler angles are computed from the elements of R_b

$$[\theta_1, \theta_2, \theta_3]^\top = [\text{atan2}(R_{b\ 3,2}, R_{b\ 2,2}),\ \text{asin}(-R_{b\ 1,2}),\ \text{atan2}(R_{b\ 1,3}, R_{b\ 1,1})]^\top \tag{5}$$

where atan2 is the four quadrant version of the inverse tangent. The body center is taken as the mean position of BCS_2 in BCS_2'. The final three translation dof are measured in BCS_2' as the translation of the BCS_2 origin from the body center.

Results show the poses during deployment are primarily a result of rotations about the joint and small translations. For correlation analysis, deployments were grouped by the angle of deployment and colored by the number of the bounce to show the decay of the motion. The location of the body center was 130 mm from the joint, yet translation was typically ±5, 2 and 1 mm in x, z and y components and showed no pattern. The lack of translation motion suggests that the boundary effects of the hinge restrict the fold location from sliding back and forth. Restriction on fold axis sliding is also supported by the low deviation from the sphere (typically less than 1 mm), as shown in Fig. 8(b). The angles had systematic behavior, as shown in Fig. 10.

The angle of deployment, θ_1, sets the linear relation of θ_2 to θ_3, found to be

$$\begin{aligned} \theta_2 &= a_0(\theta_1 - \theta_3) + (a_1\theta_1 + a_2\theta_1^2)\theta_3 \\ [a_0,\ a_1,\ a_2] &= [0.15,\ -5.2 \cdot 10^{-3}/\text{deg},\ -1.22 \cdot 10^{-4}/\text{deg}^2]. \end{aligned} \tag{6}$$

The data was randomly split into two groups with the model fit to 70% of the data and evaluated on the other 30%.

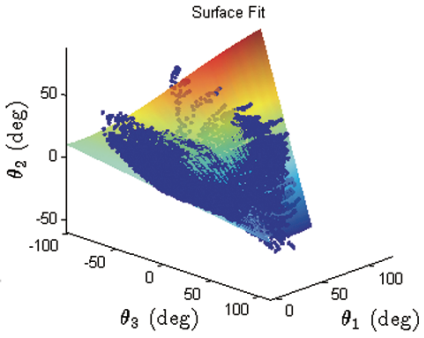

Fig. 11. Points lie very near a two dimension manifold, showing that only two independent degrees of freedom are expressed in deployment.

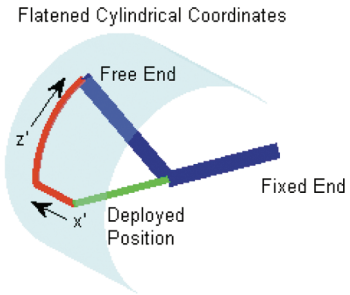

Fig. 12. To visualize the deployment envelope, the body point's x coordinate in JCS is preserved as x' while the circumference to the point is used as z'.

The correlation coefficient was 0.98 or higher for the predicted and actual θ_2 on the evaluation group. The surface and data points are shown in Fig. 11. The residuals do show cubic behavior in the residuals, but a sufficient increase in correlation could not be provided to justify the addition of a higher order term to the fit. Fits with the tangent function also provided similar average error, but were more ill conditioned and had residuals > 20° around the edge of the data set (opposed to the given fit which had residuals < 6° at the tips of the surface). Had a poor choice for the joint coordinate been chosen, such good agreement by a three parameter fit would have been very unlikely. Because the data lies on this two dimension manifold and a diffeomorphism exists, by the implicit function theorem only two dimensions are needed to describe the motion [37].

3.2. *Deployment motion characterization*

To visualize the motion and characterize the deployment path of the boom, the joint angles were transformed into a flattened, cylindrical coordinate system. A point 100 mm on the joint y axis was rotated according to the joint coordinates. This point was transferred into a flattened cylindrical coordinate system, as shown in Fig. 12. The side distance is undistorted, while the circumference to the point is used so that the path does not overlap when $\theta_1 > 90°$. Note that the radius of the cylinder decreases with increasing x', so as x' approaches 100 mm, $|z'|$ approaches 0 mm. This is desired so that the extremes in x' are still well posed in z'. These coordinates are used to show deployment paths.

The deployments were very repeatable given a similar starting point. An example is shown in Fig. 13, where only a handful of isolated points out of 13 deployments do not lie on the common path. With a deterministic function from start point to path existing, a path can be approximated by known examples. Approximating the complete path would require many outputs: one for each point on the path. Therefore a parameterized approximation is used based on a shifted, rotated ellipse with b_1 to b_4 as the fitting parameters and φ going from 0 to 2π to trace the ellipse.

$$\begin{bmatrix} z' \\ x' \end{bmatrix}(\varphi) = \begin{bmatrix} \cos(b_3) & -\sin(b_3) \\ \sin(b_3) & \cos(b_3) \end{bmatrix} \begin{bmatrix} b_1 \left(r\cos(\varphi) + \frac{e\,d}{1+e} \right) \\ r\sin(\varphi) \end{bmatrix} + \begin{bmatrix} 0 \\ b_4 \end{bmatrix}$$

$$e = \sqrt{1 - (b_2/b_1)^2}$$

$$d = \frac{b_2}{2}\sqrt{e^{-2} - 1}$$

$$r(\varphi) = \frac{e\,d}{1 - e\cos(\varphi)}. \tag{7}$$

The first two parameters control the major and minor diameters. The third parameter rotates the ellipse to a side angle while the final parameter translates the ellipse in the x' direction. This parametrization was chosen to capture features that were noticed in the bounces as independently as possible. Additional care was taken to ensure that values were well posed, such as applying a lower limit to the size of e and accounting for $b_2 > b_1$ occurrences.

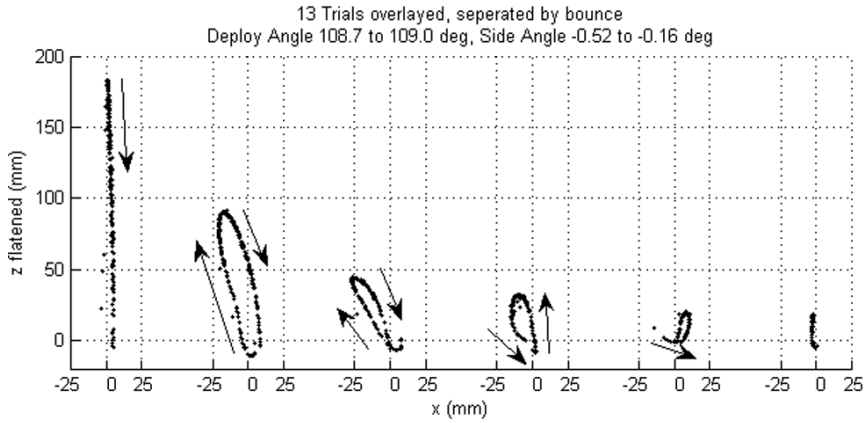

Fig. 13. With the same starting point, bounces would trace the same path. Paths are overlayed with each bounce shifted to the right, so that each bounce can be seen clearly.

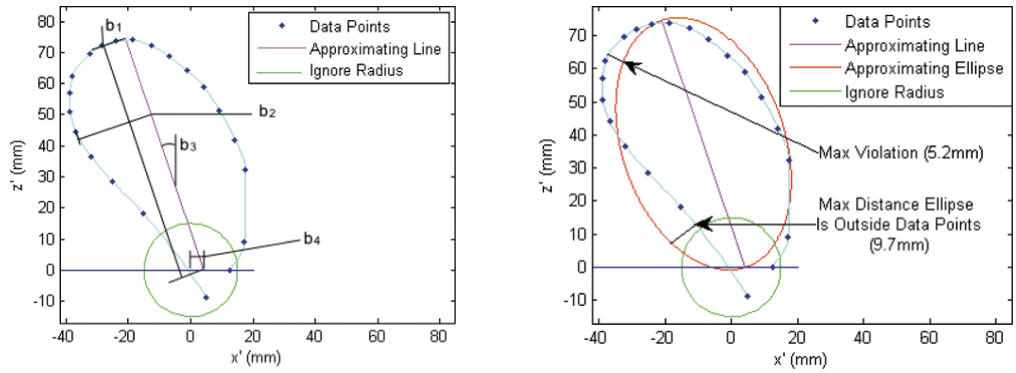

(a) Ellipse parameters (b) Performance measures

Fig. 14. Parameters for an ellipse to bound the path are derived from a line fit to the path, ignoring the path within a radius of the final location. The performance of the ellipse is by error (not bounding the path) and conservativeness (excessive distance from the path). The ellipse shape does a good job of bounding the path with a few intuitive parameters.

Parameters were generated for the first bounce of every path with significant motion. Because large scale motion is the focus of this work, paths that never exceeded 40 mm from the origin or had 5 or fewer points were dropped from the data set. A nominal clearance of 15 mm was assumed about the deployed position, so points on the path within a radius of 15 mm of the deployed position were ignored. Ignoring these points is not an excessive condition since a nominal clearance about the deployed position would be expected. The angle and offset (b_3 and b_4) were found by fitting a least squared error line, $z' = mx' + b$, based on a path interpolated between sample points to avoid bias due to the distribution of data points. The maximum distance to the path from the x' axis along the line was used for the major diameter (b_1). Twice the maximum distance from the line to the path was used for the minor diameter (b_2). An example is shown in Fig. 14. Two measures are used to evaluate the quality of the line: the maximum distance the path is outside the ellipse and the maximum distance the ellipse is outside the path. The path going outside the envelope represents a failure to bound the path, whereas the ellipse being outside the path means the envelope is excessively conservative.

This section provides the framework for analyzing the motion of specific deployments. The natural deployed motion is used to develop a coordinate system, as shown in Fig. 8. The motion of the free end does not express all four possible degrees of freedom, but lies on a 2 dimensional manifold. Flattened cylindrical coordinates, as shown in Fig. 12, are used to show how the free end moves. In these coordinates, a method is presented for characterizing the path by an ellipse, as shown in Fig. 14.

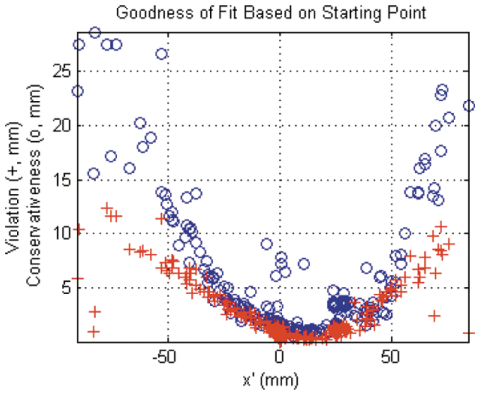

Fig. 15. Ellipses typically fit the path well, but get worse as deployments start further to the side. Violation (marked by +) is the maximum distance a data point is outside the bound, while conservativeness (marked by o) is the maximum distance for a point on the bound to the path.

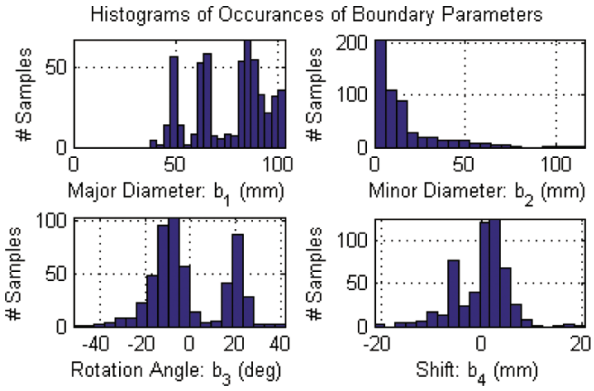

Fig. 16. The histograms for each boundary parameter of Eq. (7) shows that the scale of the error is small with respect to the scale of the fitting ellipse. Results represent 538 deployments.

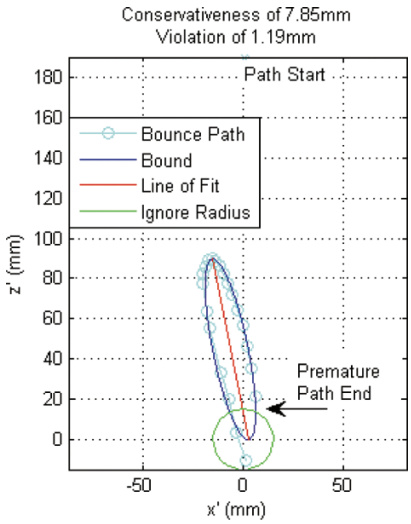

Fig. 17. The gap from the path ending before returning to the deployed position artificially increases the bounding ellipse's conservative measure.

4. Results

The goal of the analysis presented in the paper is to predict, based on the starting position, the path of a boom as it bounces after reaching the deployment position. First it will be shown that the parameterized ellipse does a good job of fitting the path and that the degradation in performance can be predicted. Then, the ellipse is compared to neighboring starting points by common area. Results show that similar starting points are a more accurate predictor than starting points further away, as would be expected. Finally, examples are shown for free-fall to show that free-free joints can be analyzed similarly.

4.1. Ellipse goodness of fit

The ellipse, described in Subsection 3.2, captured a significant portion of the true path of the bounce. Starting points near $x' = 0$ typically had great accuracy, and performance would decline quadratically with x', as shown in Fig. 15. Violations of the bounding ellipse went from 0.5 mm to 12.5 mm while the maximum distance the ellipse was outside the path went from 1.0 mm to 28.5 mm. Since the violation and conservativeness is a function of the

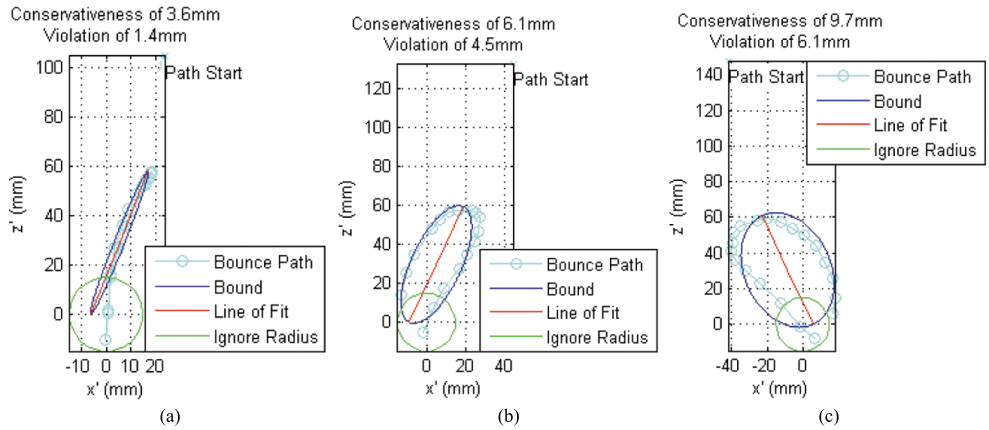

Fig. 18. The parameterized perform well for central starting points.

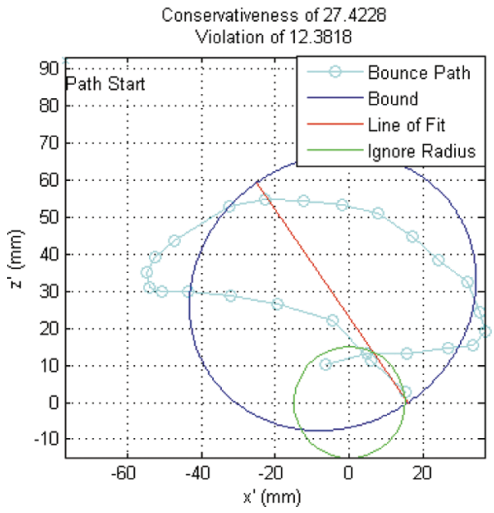

Fig. 19. For bounces with large lateral momentum, the shape of the path does not conform to the ellipse as well.

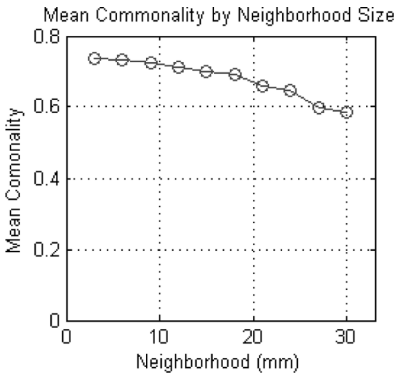

Fig. 20. The commonality of each sample to its neighbors decreases as samples from further away are included. The mean commonality drops from 74% at a 3 mm radius about the starting point to 59% at a 30 mm radius.

starting point, performance can be predicted a' priori quantitatively. This level of precision is remarkable considering the scale of motion (as shown by the ellipse fitting parameters in Fig. 16) and the seemingly unpredictable nature of a bouncing boom. There are some abberations in the results, but they arise from processing as opposed to true defects. Excessive conservativeness near $x' = 0$ was caused by the bounce path ending prior to reaching the 15 mm radius about the deployed pose where points were ignored, see Fig. 17 for an example. In these cases the ellipse forms a complete loop while the path has a gap, resulting in the conservativeness measure equaling the gap length. Typically, the gap would be within the 15 mm radius, so it would have no effect. Some typical bounding examples with low lateral momentum are show in Fig. 18. A typical example of the path with large lateral motion is shown in Fig. 19. These results do not necessarily show that this parametrization of an ellipse is poor, but that the method used to determine the parameters may not be appropriate for this type of bounce.

4.2. Prediction performance

If results are predictable, it would be expected that deployments starting from similar locations would have a similar bounding ellipse. Similarity was tested by the area common to two ellipses, scaled by the larger area. Whenever the ellipses were different, the commonality would be less than one. Because many paths had very small areas (as

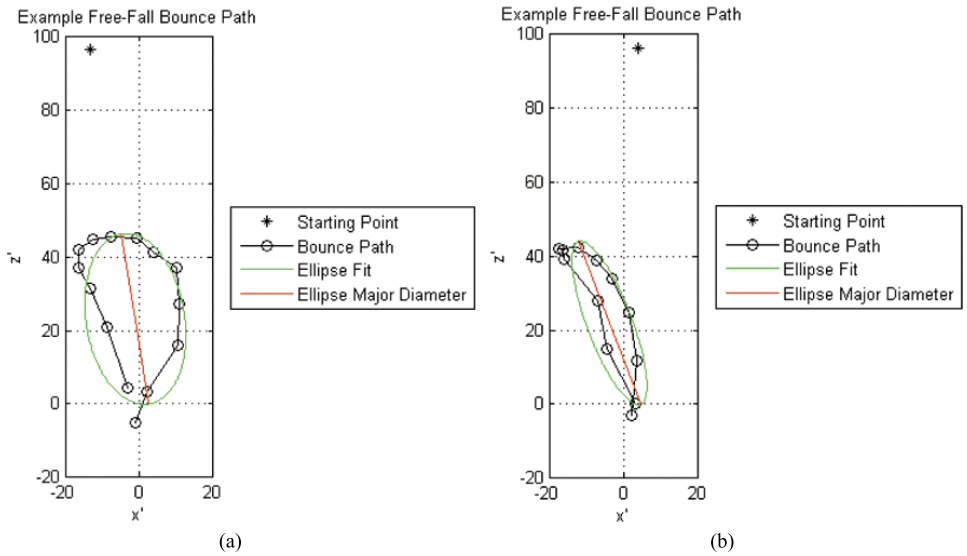

Fig. 21. The ellipse parametrization also performed well for characterizing free fall deployments.

shown by the large peak near zero in the minor diameter histogram in Fig. 16), bounding envelopes were grown by 6 mm radially to reduce the sensitivity for these very narrow ellipses.

To measure predictability, similarity of one ellipse to neighboring ellipses was measured as neighborhood size increased. The equation for commonality over a neighborhood is defined as

$$C_{i,\Psi} = \frac{\sum_{j\in\Psi} A_i \bigcap A_j}{\sum_{j\in\Psi} \max(A_i, A_j)} \tag{8}$$

where i is the sample tested, Ψ is the set of samples with starting points in the given neighborhood (not including the tested sample), A_i is the area of the extended ellipse and $A_i \bigcap A_j$ is used to capture the area of intersection of A_i and A_j. As expected, the mean of commonality drifts to lower values as the neighborhood size increases, shown in Fig. 20. Note that by weighting all neighbors in the neighborhood the same, the approximation is a zero-order model. Therefore results represent a base level of approximation and advanced prediction techniques would improve upon these results.

4.3. Free fall tests

To simulate microgravity, free-fall drop tests were preformed. Assuming the air resistance is negligible, no environmental forces will generate internal forces to the joint. The base connection was replaced by another identical pipe with both sides having videogrammetry markers. The joint coordinate system was developed as outlined in Section 3.1, with the exception that the joint motion was controlled by hand. One side is designated the free end and its motion is given in terms of the other end, as before. Accuracy of results was checked by verifying the position deviation from joint center and the manifold of Euler angles, as shown by Fig. 11.

One side of the joint was clamped 1.7 m off the floor by a structure. The joint was bent and gravity would hold the joint bent until released. By twisting the clamped end, side-angle folds were tested. The clamp was spring powered and activated by a pin released. Padding on the floor damped the impact with the floor to prevent damage between deployments. The joint would extend and bounce with in about 0.25 sec, well before hitting the padding. The ellipse parametrization preformed similar to fixed end testing. Representative results are shown in Fig. 21.

4.4. Summary

The results presented show that the ellipse does a good job at bounding the path; especially for paths with small, initial lateral deflection. As neighboring starting points approach a test starting point, their paths provide better

approximations of the path for the test point. This suggests that there is a underlying relationship of start point to deployment bounce path. Free-fall tests, simulating microgravity deployment, show elliptical motion similar to deployments using the test stand.

5. Conclusion

Tape springs can satisfy the need for deployable booms on small satellites. Low stiffness during deployment leads to large scale motion which affects stiffness. High stiffness as the cross section achieves its undeformed shape causes singularity conditions. Both of these are a challenge for analytical and finite element methods. This work addressed the possibly of predicting the large scale motion by empirical tests and provides a framework for analysis.

Results show that the path traced by a bouncing boom is repeatable. A joint coordinate system is developed from empirical data and is justified based on joint direction stiffnesses. From this coordinate system, unforced deployments clearly show two degree of freedom movements. Deployment is decomposed into a flattened cylindrical coordinate system for the benefit of a convenient visualization of the extents of the path and can be used to identify possible collisions and binding. Results are directly applicable to isolated tape spring joints. Combinations of tape springs will have the same or less expressed degrees of freedoms, 1 or 2 dof, so the analysis presented is applicable. Systems with only 1 dof would be expected to have degenerate ellipses, but performance on either case cannot be predicted based on this set of tests.

The bound of the path is well described by an ellipse; whose major and minor diameters, rotation and offset are determined by the path. Results show the ability to restrict violations beyond the predicted envelope from 0.5 to 12.5 mm, based on the starting lateral deflection. This accuracy is good, considering the bounces are 50–100 mm large at angles to the side up to 50 degrees. These bounds are also not excessively conservative, with the maximum distance from the envelope to the path being 1 to 29 mm, also predicted by the starting lateral deflection. There is evidence that bounding ellipses of neighboring starting points can be used to predict the bounding ellipse of a novel starting point. A comparison by common area shows that deployments with closer starting points have more in common than distant points. This is a zero-order evaluation and is shown as a baseline of what accuracy can be obtained. Free-fall deployments test a free-free condition and show similar behavior. This shows that the analysis also applies to deployments in space.

The methodology in this work provides a foundation for analysis and design of large, complicated deployments. Results specifically address symmetric boom inertia. Components attached to the boom, such as sails, panels or antenna, will likely affect the bound of the deployment path. Further investigation would be needed to address off-centered or flexible boom payloads. First, the results show that the path a boom bounces can be predicted, though bounces appear chaotic and are ill-conditioned for analysis. The coordinate systems and parameterizations presented allow for a parsimonious representation so that future analysis is as simple as possible. Data can be compiled for sets of joints to allow for interpolation between starting position (and possibly velocities), joint parameters, boom mass and other factors. This database would allow for estimation of deployment paths for preliminary designs, reducing the need for large-scale, finite-element analysis and prototype testing until the initial design has been refined.

Acknowledgments

We would like to thank the Air Force Research Laboratory and the Air Force Office of Scientific Research for funding support. We would also like to thank Dr. Ronald Tuttle of the Physics Department for hardware and laboratory support and Mr. Daniel Magree of Georgia Tech, Mr. Thomas Hunt Pace of Virginia Military Institute, Alexander T. Trinh of Trinity University for exploratory testing and programming.

References

[1] A. Toorian, K. Diaz and S. Lee, The cubesat approach to space access, in: *Aerospace Conference, 2008 IEEE* (2008), 1–14, doi:10.1109/AERO.2008.4526293.

[2] H. McGinnis, S. Lee, S. Smith, E. Flint and J. Lindler, Videogrammetric quantification of deployment behavior of rollable membrane shell technology apertures, in: *Structures, Structural Dynamics, and Materials Conference*, Orlando, Florida, 2010, doi:10.2514/6.2010-2833.
[3] O. Soykasap, A. Watt and S. Pellegrino, New deployable reflector concept, in: *Structures, Structural Dynamics, and Materials Conference*, Palm Springs, California, 2004, doi:10.2514/6.2004-1574.
[4] P.W. Chung and E.A. Thornton, Torsional buckling and vibrations of a flexible rolled-up solar array, in: *Structures, Structural Dynamics, and Materials Conference*, New Orleans, Louisiana, 1995.
[5] K.A. Seffen, Z. You and S. Pellegrino, Folding and deployment of curved tape springs, *International Journal of Mechanical Sciences* **42**(10) (2000), 2055–2073, doi: 10.1016/S0020-7403(99)00056-9.
[6] J.L. Domber, J.D. Hinkle, L.D. Peterson and P.A. Warren, The deployment repeatability of a high stiffness folded composite hinge, in: *Structures, Structural Dynamics, and Materials Conference*, Seattle, WA, 2001.
[7] R. Cobb, J. Black and E. Swenson, Design and flight qualification of the rigidizable inflatable get-away-special experiment, *Journal of Spacecraft and Rockets* **47**(4) (2010), 659–669, doi: 10.2514/1.48636.
[8] J.L. Domber, J.D. Hinkle, L.D. Peterson and P.A. Warren, Dimensional repeatability of an elastically folded composite hinge for deployed spacecraft optics, *Journal of Spacecraft and Rockets* **39**(5) (2002), 646–652, doi: 10.2514/2.3877.
[9] J.T. Black, R.G. Cobb, E.D. Swenson and B.J. Cooper, Rigidizable inflatable get-away-special experiment space flight data analysis, *Journal of Spacecraft and Rockets* **48**(3) (2011), 477–487, doi: 10.2514/1.50939.
[10] R. Kumar and S. Ahmed, Some boom choices for design of deployable solar arrays, *Solar Energy* **16**(3–4) (1974), 159–163, doi: 10.1016/0038-092X(74)90013-9.
[11] S. Ahmed, R. Kumar and R. Predmore, Predictions of solar induced response of thin walled open section booms for design, *Proceedings of the International Symposium on Experimental Mechanics* **1** (1972), 1–14.
[12] R. Crawford, Strength and efficiency of deployable booms for space applications, in: *Variable Geometry and Extendible Structures Conference*, Anaheim, California, 1971.
[13] S.K. Jeon and T.W. Murphey, Design and analysis of a meter-class CubeSat boom with a motor-less deployment by bi-stable tape springs, in: *Structures, Structural Dynamics, and Materials Conference*, vol. AIAA-2011-1731, Denver, Colorado, 2011.
[14] S.J.I. Walker, A.D. McDonald, T. Niki and G.S. Aglietti, Initial performance assessment of hybrid inflatable structures, *Acta Astronautica* **68**(7–8) (2011), 1185–1192, doi: 10.1016/j.actaastro.2010.10.009.
[15] M. Straubel, J. Block, M. Sinapius and C. Hühne, Deployable composite booms for various gossamer space structures, in: *Structures, Structural Dynamics, and Materials Conference*, vol. AIAA-2011-2023, Denver, Colorado, 2011.
[16] M.E. McEachen, Development of the GEMS telescope optical boom, in: *Structures, Structural Dynamics, and Materials Conference*, Denver, Colorado, 2011.
[17] E.H. Mansfield, Large-deflexion torsion and flexure of initially curved strips, *Proceedings of the Royal Society of London, A Mathematical and Physical Sciences* **334**(1598) (1973), 279–298, doi: 10.1098/rspa.1973.0092.
[18] K.A. Seffen, On the behavior of folded tape-springs, *Journal of Applied Mechanics* **68**(3) (2001), 369–375, 2000, doi: 10.1115/1.1365153.
[19] M. Silver, J. Hinkle and L. Peterson, Modeling of snap-back bending response of doubly slit cylindrical shells, in: *Structures, Structural Dynamics, and Materials Conference*, vol. AIAA-2004-1820, Palm Springs, California, 2004, doi: 10.2514/6.2004-1820.
[20] S.J.I. Walker and G. Aglietti, Study of the dynamics of three dimensional tape spring folds, *AIAA Journal* **42**(4) (2004), 850–856, doi:10.2514/1.908.
[21] S.J.I. Walker and G. Aglietti, Study into the dynamics of three dimensional tape spring folds, in: *Structures, Structural Dynamics, and Materials Conference*, Norfolk, Virginia, 2003, 10.2514/6.2003-1499.
[22] H. Mallikarachchi and S. Pellegrino, Design and validation of thin-walled composite deployment booms with tape-spring hinges, in: *Structures, Structural Dynamics, and Materials Conf*, Denver, Colorado, 2011.
[23] M. Leipold, M. Eiden, C. Garner, L. Herbeck, D. Kassing, T. Niederstadt, T. Krüger, G. Pagel, M. Rezazad, H. Rozemeijer, W. Seboldt, C. Schöppinger, C. Sickinger and W. Unckenbold, Solar sail technology development and demonstration, *Acta Astronautica* **52**(2–6) (2003), 317–326, doi:10.1016/S0094-5765(02)00171-6.
[24] A.M. D'Amato, B.J. Arritt, J.A. Banik, E.V. Ardelean and D.S. Bernstein, Structural health determination and model refinement for a deployable composite boom, in: *Structures, Structural Dynamics, and Materials Conf*, Palm Springs, California, 2009, doi: 10.2514/6.2009-2373.
[25] S.J.I. Walker and G.S. Aglietti, Experimental investigation of tape spring folded in three dimensions, *AIAA Journal* **44**(1) (2006), 151–159, doi: 10.2514/1.15508.
[26] Y. Liu, S. Kim, A. Chattopadhyay and D. Doyle, Application of system identification techniques to health monitoring of on-orbit satellite boom structures, *Journal of Spacecraft and Rockets* **48**(4) (2011), 589–598, doi: 10.2514/1.51818.
[27] F. Beavers, N. Munshi, M. Lake, A. Maji, B.C.K. Qassim and S. Rawal, Design and testing of an elastic memory composite deployment hinge for spacecraft, in: *Structures, Structural Dynamics, and Materials Conference*, Denver, Colorado, 2002, doi: 10.2514/6.2002-1452.
[28] W. Francis, M. Lake, K. Mallick, G. Freebury and A. Maji, Development and testing of a hinge/actuator using elastic memory composites, in: *Structures, Structural Dynamics, and Materials Conference*, Norfolk, Virginia, 2003, doi: 10.2514/6.2003-1496.
[29] O. Soykasap, Analysis of tape spring hinges, *International Journal of Mechanical Sciences* **49**(7) (2007), 853–860, doi: 10.1016/j.ijmecsci.2006.11.013.
[30] S.J.I. Walker and G.S. Aglietti, Modeling the hinge moment of skew-mounted tape spring folds, *Journal of Aerospace Engineering* **20**(2) (2007), 102–115, doi: 10.1061/(ASCE)0893-1321(2007)20:2(102).
[31] G.M. Olson, T. Murphey and G. Thomas, Free deployment dynamics of a Z-folded solar array, in: *Structures, Structural Dynamics, and Materials Conference*, Denver, Colorado, 2011.
[32] M. Santer, A. Sim and J. Stafford, Testing of a segmented compliant deployment boom for cubesat magnetometer missions, in: *Structures, Structural Dynamics, and Materials Conf*, Denver, Colorado, 2011.

[33] J.N. Footdale, J.A. Banik and T.W. Murphey, Design developments of a non-planar deployable structure, in: *Structures, Structural Dynamics, and Materials Conf*, Orlando, Florida, 2010, doi: 10.2514/6.2010-2608.
[34] D. Adams and M. Mobrem, Analysis of the lenticular jointed MARSIS antenna deployment, in: *Structures, Structural Dynamics, and Materials Conference*, Newport, Rhode Island, 2006, doi: 10.2514/6.2006-1683.
[35] F.A. Roybal, J.A. Banik and T.W. Murphey, Development of an elastically deployable boom for tensioned planar structures, in: *Structures, Structural Dynamics, and Materials Conf*, Honolulu, Hawaii, 2007, doi: 10.2514/6.2007-1838.
[36] D. Magree, J. Black, A. Jennings, G. Briggs and C. Allen, Pan-tilt-zoom hybrid camera system for dynamic tracking and measurement, *AIAA Journal* **49**(9) (2011), 1988–1999, doi: 10.2514/1.J050990.
[37] J. Stewart, Calculas, 4th Edition, Brooks/Cole Publishing Co., Pacific Grove, Ch. 15, Partial Derivatives, CA, 1999, 956–957.